Corrosion and mechanical assessment in $LiNO_3$ molten salt as thermal energy storage material in CSP plants

Abdiel Mallco[1], Angel G. Fernandez[2], Johannes Preußner[3], Carlos Portillo[1]

[1] Centro de Desarrollo Energético Antofagasta (CDEA), Universidad de Antofagasta, Antofagasta (Chile)

[2] GREiA Research Group, INSPIRES Research Centre, Universitat de Lleida, Lleida (Spain)

[3] Fraunhofer – Institute for Mechanics of Materials IWM, Freiburg (Germany)

Abstract

The development of solar thermal energy in Chile, leads to the realization of applied research in such a way that new technologies and applications suitable to the conditions of the Atacama Desert can be proposed. In view of the search for new fluids feasible to be applied in CSP technology as thermal energy storage using molten salts, this research proposes the use of the mixture composed by 30wt. % $LiNO_3$ – 13wt. % $NaNO_3$ – 57wt. % KNO_3. Corrosion has been evaluated on different stainless steels (AISI430, AISI304, VM12-SHC) and a Ni base alloy (HR-224). In order to monitorize corrosion, electrochemical impedance spectroscopy and linear polarization technique have been applied in order to obtain the corrosion rate and the corrosion mechanism as well. The corrosion rates obtained for AISI304, AISI430, VM12 and HR224 was 1.82, 2.69, 3.53 and 0.63 (mm/year), respectively at 550°C and 100 h of immersion.

Finally, the effect of molten salts on the mechanical properties of materials used in solar thermal plants is studied, as well as the effect of Flow Accelerated corrosion (FAC), determining the most suitable methods for these evaluations.

Keywords: Molten Salts; Corrosion; Mechanical Properties; Electrochemical impedance spectroscopy; FAC (Flow Accelerated Corrosion)

1. Introduction

The last two and a half centuries of human development on earth, has been shown that our species depends almost entirely on fossil fuels within its energy needs. Coal, oil and gas are finite resources that we have chosen to extract at an extremely high rate to sustain our growing demand for energy. This strong dependence on fossil fuels leads to an alarming increase in CO_2 emissions, which implies the accelerated global warming of our planet (Green, Diep, Dunn, & Dent, 2015; Starke, Cardemil, Escobar, Lemos, & Colle, 2015).

Given these situations, the solution seems to be in a different technological change that relates the generation of energy with the efficient use of it, increasing production technologies with low CO_2 emissions (Solar, Hydraulic, Wind, etc.). Given this, one of the challenges found in the generation of electric power, is the use of Concentrated Solar Power (CSP) technology with Thermal Energy Storage (TES).

CSP has a relatively high number of distinct components, making it a complicated technology. This drawback, however, is offset by the fact that the technology offers versatility in application to suit demand. The conversion initially to thermal energy differentiates CSP from the other major renewable energy technologies such as hydropower, wind power and PV (Gauché et al., 2017). CSP plants use mirrors to focus sunlight and produce high-temperature thermal energy that can be stored inexpensively. This feature allows CSP to be a dispatchable electricity resource available whenever there is customer demand, including at times when the sun is not shining. CSP with thermal energy storage (TES) presents an economic advantage if it supplies electricity at times of greatest need which generally has the highest electricity tariff (Stekli, 2013). The system currently used in CSP plants, is based on the storage of sensible heat that consists of storing the heat at high temperature using nitrate based molten salts, to subsequently release this stored heat by a decrease in temperature of the material.

Molten salts have a great application as a heat transfer fluid (HTF) in concentration solar power (CSP) plants , reaching excellent results in conventional power generation plants (McConohy & Kruizenga, 2014). Today most advanced CSP systems are towers integrated with two-tank molten-salts TES, delivering thermal energy at 565 °C for its integration in conventional steam-Rankine power cycles (Mehos et al., 2017).

doi:10.18086/swc.2019.21.04 Available at http://proceedings.ises.org

The materials used in the CSP technology are exposed to very high corrosion due to the high operation temperature. Molten-salts corrosion attack can occur by different mechanisms, but quantitative data for materials selection and performance prediction using commercial nitrate salts are rarely available, and corrosion mechanisms are related with the different anions and cations in the molten salts system.(Á. G. Fernández & Cabeza, 2019).

Several studies have demonstrated the corrosive effects at high temperature of the molten salts in different alloys with high noble metal contents, mainly producing the dissolution of the alloys (Bradshaw & Goods, 2001). The most commonly used materials in this type of technology include carbon steels, stainless steels and nickel-based alloys. One of the main focuses of the research and development of molten salts is the corrosion in the materials most used at high temperatures for solar applications and its mitigation to obtain degradation of containment materials lower, thus providing a lifetime for CSP plants of 30 years or more.

Molten salt currently used in CSP plants as energy storage material is the binary mixture 60% $NaNO_3$ + 40% KNO_3 (solar salt) (A. G. Fernández, Galleguillos, & Pérez, 2014), allowing up to 15 hours of thermal energy storage. Recent studies have proposed a nitrate salt with a composition of 30wt.% $LiNO_3$ – 13wt.% $NaNO_3$ – 57wt.% KNO_3 (Cheng, Chen, & Wang, 2015), this mixture would allow better working ranges and outstanding thermal properties with respect to solar salt. Based on this mixture, the present investigation proposes the monitoring of the corrosion process by electrochemical impedance spectroscopy (EIS) and the analysis of the corrosion activity by the technique of electrochemical polarization.

EIS is a powerful monitoring technique that is widely used in fields as diverse as energy and other areas. EIS data can be used to obtain physical properties, such as diffusion coefficients and chemical reaction rates, and microstructural characteristics of the electrochemical system under study. The implementation of an EIS experiment is relatively simple (Ciucci, 2019).

Electrochemical polarization and electrochemical impedance spectroscopy (EIS) tests provide information on the corrosion rate as well as provide information on the kinetics of the corrosion process that helps to identify the different anodic and cathodic reactions. They also help to identify the different materials that are susceptible to corrosion under specific conditions.

The electrochemical polarization technique analyses the metal/electrolyte interface, where it measures the electric current generated by an externally applied potential. Electrochemical impedance spectroscopy (EIS) uses a small voltage signal between different amplitudes over an equilibrium potential or another known potential, which causes the induced current to be measured while the voltage is modulated in different frequency ranges. The different values obtained by the polarization technique are represented by the cathodic and anodic curve from which the corrosion potential and the corrosion current can be obtained; with these values, the corrosion rate of the material immersed in the molten salt can be obtained. (Ciucci, 2019; Gomez-Vidal, Fernandez, Tirawat, Turchi, & Huddleston, 2017).

The present investigation also analyses the corrosion and erosion activity produced by the flow accelerated corrosion (FAC). The material degradation in carbon steel piping systems produced by the FAC represents one of the major problems in many industries including CSP, because of its detrimental effect on various piping components. It is widely known that the severe FAC damage normally occurs in tees, elbows, downstream of control valves, flow elements, reducers or orifices. The wall thinning caused by FAC in piping systems may lead to catastrophic failures of system components and may also result in serious fatalities. The pipe wall thinning rate due to FAC depends on a complex interaction of several parameters such as material composition, water chemistry, and hydrodynamic (Ahmed, 2010).

The exposure of materials to molten nitrate salts normally results in a loss of ductility and/or a reduction in strength, that is why this research finally proposes the analysis of the effect of the molten salt on the loss of the mechanical properties of the materials used in the CSP industry by the technique of slow strain rate tensile SSRT.

The effect of salt exposure on mechanical properties of alloys can be evaluated by means of a constant extension rate tensile (CERT) test. The CERT, also called slow strain rate tensile (SSRT) test, is a standard testing method in which the specimen is subjected to a constant elongation rate. Cyclic mechanical loading with plastic deformation leads to micro-crack formation, which occur early in the lifetime of a component. The lifetime of a component, which is subjected to low cycle fatigue (LCF) loads, is then determined by the growth rate of these micro-cracks. The presence of a corrosive environment can accelerate the crack growth and thus reduce the component life. This effect can be particularly detrimental in pipe systems of concentrated solar power plants like central receivers or heat exchangers, where apart from the contact with a corrosive high temperature fluid, the materials are subjected to thermal fluctuations and mechanical loads (Preußner et al., 2016).

2. Material and Methods

2.1. Preparation of salt mixture

The nitrate salts mixtures used for this research are KNO_3, $LiNO_3$ and $NaNO_3$ (refined over 99% purity). In the first instance, this mixture of salts was introduced in an alumina crucible in an oven at different heating temperatures and exposure times, such as 100 (3h), 200 (3h), 350 (2h) and 550 (2h) °C, in order to remove corrosive impurities in the salt mixture. Once the mixture of salts reached the temperature of 550°C, it was maintained this temperature during 24h, to homogenize before the corresponding tests.

2.2. Preparation of samples for electrochemical impedance and spectroscopy Polarization tests

The samples of stainless steel have the dimensions of AISI304 (2 mm x 20 mm x 10 mm), AISI430 (2 mm x 20 mm x 10 mm), VM12_SHC (2 mm x 12 mm x 10 mm) and nickel allow HR224 (2mm x 20mm x 10mm). The compositions of materials tested are shown in Table 1.

Table 1: Chemical composition of 304, 430 Stainless Steel and HR-224 alloy nickel

Samples	wt.%									
	Si	**Mn**	**Cr**	**P**	**Mo**	**C**	**S**	**Ni**	**Fe**	**Others**
304	0.75 max	2 max	18 - 20	0.045 max	-	0.08 max	0.03 max	8-10.5	Balance	2 Co, 0.5 W, 0.15 Nb, 3.8 Al.
T91	0.5	0.6	9.5	0.02	1.05	0.12	0.01	-	Balance	-
430	1 max	1-1.25	16 - 18	0.06 max	-	0.12 max	0.03 max	-	Balance	-
VM12	0.4	0.45	12.0	-	0.2	0.1	-	0.4	Balance	1.8 Co, 0.3 V, 1.7 W, 0.25 Cu.
HR-224	0.3	0.5 max	20	-	0.5 max	0.05	-	Balance	27.5	-

Samples for Electrochemical Impedance Spectroscopy were welded using a Ni-Cr wire of diameter about 0.95 mm. The working electrode sample (WE) and the counter electrode (CE) were introduced into an alumina tube and sealed with high temperature castable cement. The pseudo-electrode of reference (RE) was auto-circuited with the counter electrode (CE) for the electrochemical tests with the potensiostat (AUTOLAB-PGSTAT302N). Figure 1 shows the scheme of the electrochemical test. The values of the parameters for the electrochemical impedance test were obtained in a frequency range between 100 [KHz] and 10 [mHz]. Polarization tests were carried out between the potentials of -0.6 to 0.4 [V] of the OCP (open circuit potential) voltage. The scanning range is 0.001 [V/s] with steps of 0.00244 [V].

2.3. Preparation of samples for slow strain rate tensile (SSRT) tests

The effect of the exposure of the salts on the mechanical properties and their influence on the fracture of the material has been evaluated. For a proper SSRT test, the experimental arrangement shown in figure 2 has been used. The reactor has a volume of 10 liters and the maximum load capacity of the equipment is 150 kN. The materials evaluated with this technique were T91 and VM12 steels, with the chemical composition showed in table 1.

2.4. Preparation of samples for Flow Acceleration Corrosion (FAC)

The flow accelerated corrosion (FAC) tests were performed in comparison with mass gain corrosion tests, in which the material used for both tests was T91, where the samples used in both cases were transverse cuts of 1 inch diameter pipes with a longitudinal section of approximately 32 mm. The cross sections for the FAC test are predisposed in such a way that they can simulate the effect of the fluid of the molten salts in movement through an agitator connected to an electric motor. The agitation speed in the FAC system was performed at a speed of 300 rpm. The test was performed on the mixture of ternary salt with proposed lithium content at 550 °C up to an exposure time of 624 hours. Similarly, the same tests were performed in stationary mode to see the influence of FAC on static corrosion; the exposure time in this case was 696 hours. Figure 3 shows the FAC configuration system for the tests performed.

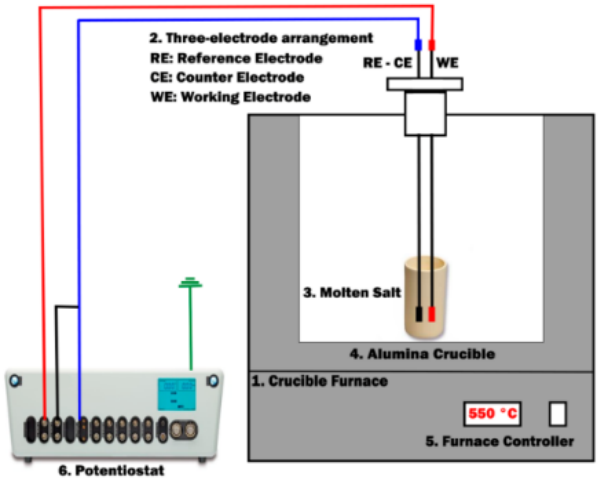

Fig. 1: Schematic of the electrochemical system: 1: Crucible furnace; 2: Two-electrode arrangement (Re: reference electrode/CE: counter electrode and WE: working electrode); 3: molten salt; 4: alumina crucible; 5: furnace controller; 6: Potentiostatic

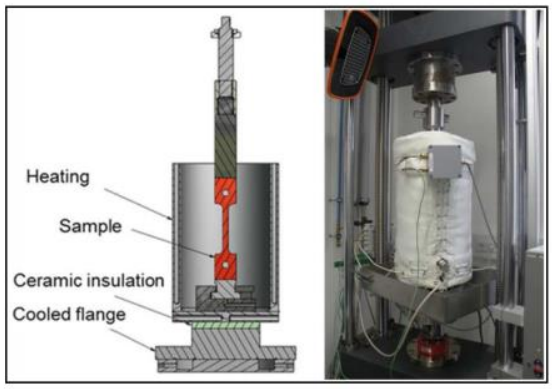

Fig. 2: Assembly of the SSRT tests

Fig. 3: Assembly of Flow Acceleration Corrosion test and corrosion by gravimetry

3. Results

3.1. Electrochemical impedance spectroscopy and polarization technique

Figure 4 shows the different Nyquist diagrams for stainless steel AISI304, AISI430, VM12 and a Ni base alloy HR-224 in salt of lithium content (57 wt.%K, 30wt.%Li, 13wt.%Na)NO_3. Measurement times were carried out at 2, 4, 6, 8, 24, 48, 72 and 96 hours of exposure in molten salts. The impedance spectra for the corrosion process of samples in contact with salt of lithium content are very similar throughout the experimental process. The equivalent circuit characteristic for all figures are composed of two capacitive-resistive circuits connected in parallel, in addition to both connected in series to a resistance. According to the different models of corrosion in molten salts, the equivalent

circuit corresponds to the formation of a protective layer in active metals (Zeng, Wang, & Wu, 2001).

According to the graphs of the impedance spectra for molten salt with lithium content for all samples, they show that the corrosion process is controlled by the transfer of ions in the protective layer as shown in Figure 5, which is consistent since the tests were carried out in the first hours of contact between the metal and the molten salt, this because they represent the most significant hours of the corrosion process.

For this model of protective layer, the transport of ions in the protective layer can limit the corrosion rate. The different elements that comprise the protective layer equivalent circuit are represented by the following elements: R_s is the resistance of the molten salts, C_{dl} is the double layer capacitance at the metal / salt-melted interface and R_t is the transfer resistance electrochemistry. Often the behaviour of the capacitors in the EIS tests is not the most ideal, so instead a constant phase element acts for the adjustments of the experimental data. R_{ox} represents the transfer resistance of ions in the scale and $C_{ox}$is the oxide capacitance. So, for this equivalent circuit may be expressed by equation 1:

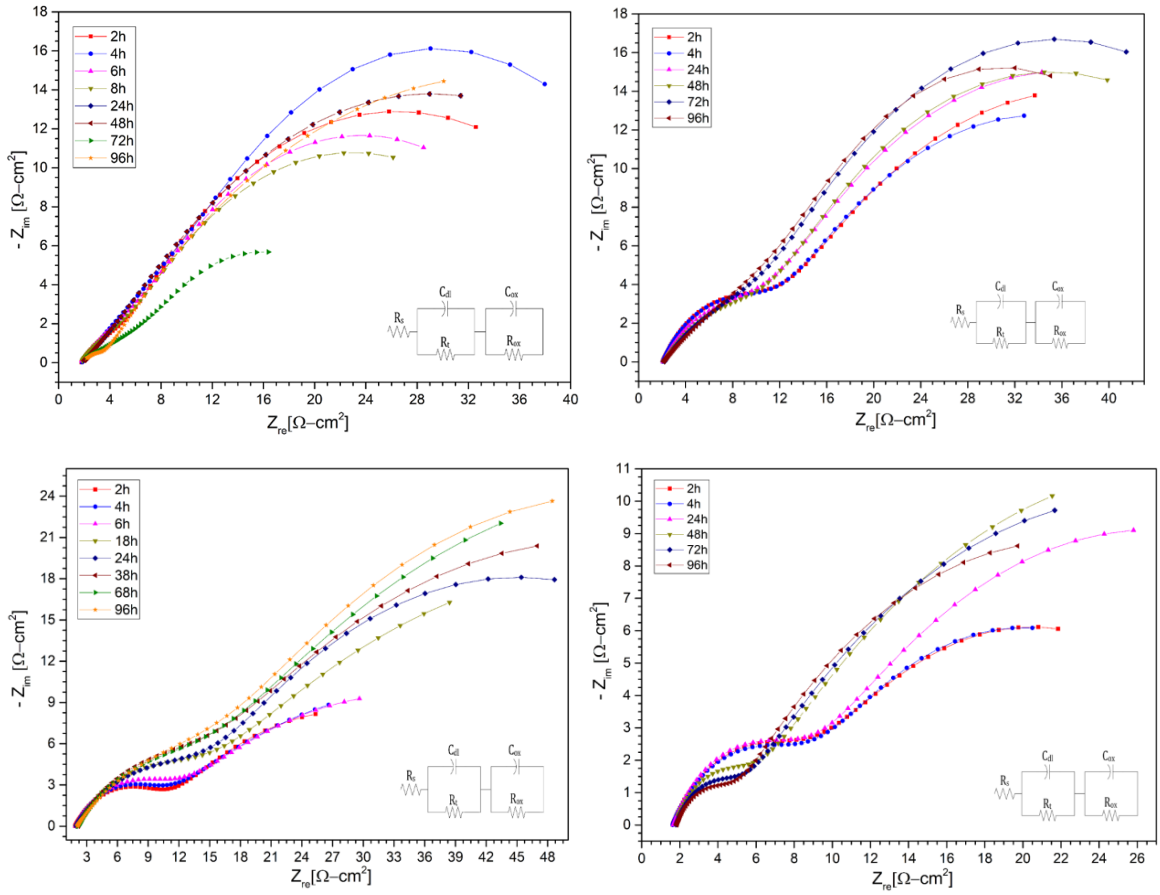

Fig. 4. Nysquist diagram of the samples in $KLiNaNO_3$ (ternary salt with lithium content) at 100h and 550°C a) AISI304, b) AISI430, c) VM12 and d) HR-224

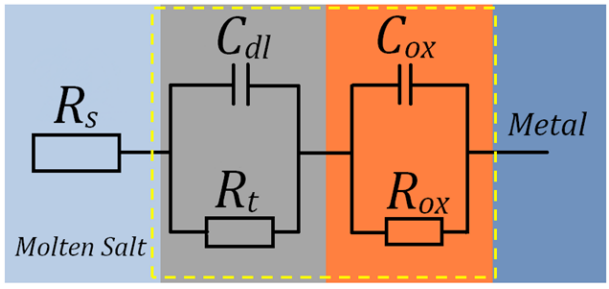

Fig. 5 Equivalent circuit representing the corrosion of metals forming a protective scale in molten salts

$$Z = R_s + \frac{1}{jwC_{dl} + wC_{dl}\cot\left(\frac{\beta_{dl}\pi}{2}\right) + \frac{1}{R_t}} + \frac{1}{jwC_{ox} + wC_{ox}\cot\left(\frac{\beta_{ox}\pi}{2}\right) + \frac{1}{R_{ox}}} \qquad (eq.1)$$

where, β_{dl} and β_{ox} represents the dispersion coefficient the first and second capacitance of the circuit, respectively. Therefore, $wC_{dl}\cot\left(\frac{\beta_{dl}\pi}{2}\right)$ and $wC_{ox}\cot\left(\frac{\beta_{ox}\pi}{2}\right)$ are the elements of the impedance caused by the dispersion effect. Because corrosion is controlled by the transport of species in the protective layer, the radius of the second capacitance circuit must be greater than that of the first cycle. In addition, in this case, the corrosion resistance of the metals in the molten salts can be represented by the R_{ox} parameter.

The materials studied present an excellent protection against corrosion that can be verified with the results obtained in the adjustments of tables 2 to 5, specifically in the model formed by a protective layer.

Table 2: Fitting results of the impedance spectra of stainless steel 304 during corrosion in the presence of $KLiNaNO_3$ (ternary salt with lithium content) at 550 °C.

Time	R_s	C_{dl}	β_{dl}	R_t	C_{ox}	β_{ox}	R_{ox}
	Ω-cm²	F s^(β_dl-1)		Ω-cm²	F s^(β_ox-1)		Ω-cm²
2 h	1.778	0.036	0.55	3.9	0.11	0.696	42.1
4 h	1.850	0.07263	0.4498	32.21	0.3564	0.961	21.7
6 h	1.707	0.1801	0.7652	32.13	0.06792	0.4847	7.229
8 h	1.768	0.162	0.7038	34.08	0.06122	0.5094	4.783
24 h	1.822	0.1305	0.3687	19.38	0.1734	0.7076	35.11
48 h	1.822	0.1734	0.7076	35.11	0.1305	0.3687	19.38
72 h	1.533	1.345	0.8879	5.228	0.1434	0.2281	109.6
96 h	1.953	0.095	0.5534	63.62	0.011	0.5297	1.574

Table 3: Fitting results of the impedance spectra of stainless steel 430 during corrosion in the presence of $KLiNaNO_3$ (ternary salt with lithium content) at 550 °C.

Time	R_s	C_{dl}	β_{dl}	R_t	C_{ox}	β_{ox}	R_{ox}
	Ω-cm²	F s^(β_dl-1)		Ω-cm²	F s^(β_ox-1)		Ω-cm²
2 h	2.047	0.14	0.625	52	0.012	0.62	10
4 h	2.049	0.142	0.692	42.94	0.01279	0.6152	10.23
24 h	2.098	0.02	0.56	9.7	0.15	0.68	50.00
48 h	2.221	0.02481	0.5301	10.1	0.19	0.71	47.56
72 h	2.194	0.0414	0.48	12.35	0.23	0.77	46.87
96 h	2.074	0.062	0.41	22.78	0.43	0.91	28.36

Table 4: Fitting results of the impedance spectra of Nickel alloy HR224 during corrosion in the presence of $KLiNaNO_3$ (ternary salt with lithium content) at 550 °C.

Time	R_s	C_{dl}	β_{dl}	R_t	C_{ox}	β_{ox}	R_{ox}
	Ω-cm²	F s^(β_dl-1)		Ω-cm²	F s^(β_ox-1)		Ω-cm²
2 h	1.617	0.016	0.634	7.2	0.21	0.59	24
4 h	1.617	0.0018	0.63	7.2	0.26	0.61	23
24 h	1.664	0.012	0.67	6.8	0.169	0.58	37
48 h	1.745	0.15	0.56	47	0.013	0.718	3.75
72 h	1.799	0.015	0.7	3.17	0.18	0.56	4.3
96 h	1.83	0.0183	0.677	2.9	0.21	0.59	3.5

Table 5: Fitting results of the impedance spectra of VM12 during corrosion in the presence of $KLiNaNO_3$ (ternary salt with lithium content) at 550 °C.

Time	R_s	C_{dl}	β_{dl}	R_t	C_{ox}	β_{ox}	R_{ox}
	Ω-cm^2	F s^(β$_{dl}$-1)		Ω-cm^2	F s^(β$_{ox}$-1)		Ω-cm^2
2 h	1.874	0.0083	0.54	37.5	0.195	0.64	8.7
4 h	1.918	0.0081	0.68	54.3	0.146	0.45	7.6
6 h	1.920	0.0089	0.65	47.4	0.137	0.49	9.2
18 h	2.069	0.0133	0.63	84.7	0.122	0.53	11.5
24 h	2.158	0.0110	0.68	64.3	0.125	0.58	14.7
38 h	2.161	0.0178	0.62	76.81	0.135	0.62	13.2
68 h	2.167	0.0217	0.69	95.13	0.126	0.61	12.8
96 h	2.169	0.0464	0.71	75.45	0.125	0.54	17.3

Linear polarization results are shown in figure 6, obtaining the corrosion parameters shown in table 6. The relationship between the corrosion rates of the molten salt of the study can be observed taking into account the open circuit potential of the electrochemical system, the corrosion potential and the current density.

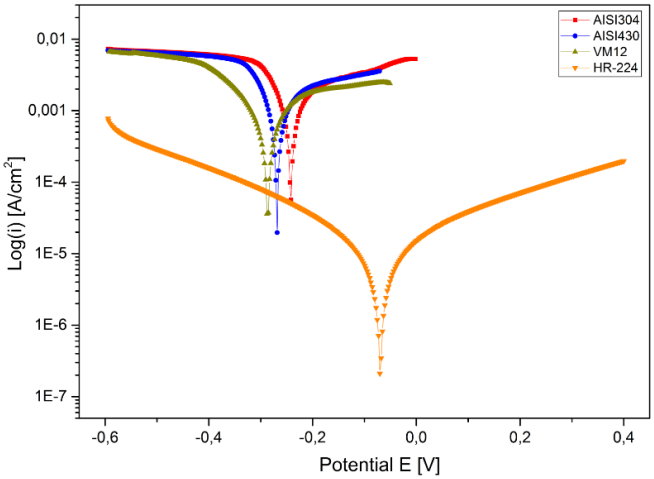

Fig.6. Polarization curves of samples in $KLiNaNO_3$ (ternary salt with lithium content) at 550°C

Table 6: Corrosion data of tested 304, 430, VM12 and HR-224 in $KLiNaNO_3$ (ternary salt with lithium content) at 550 °C.

Sample	OCP (mV)	E_{corr} (mV)	j_{corr} (µA/cm^2)	CR (mm/year)
304 (lithium)	0.24	-242.28	224.10	1.82
430 (lithium)	2.20	-268.69	254.42	2.69
HR-224 (lithium)	-4.17	-169.34	208.30	0.63
VM12 (lithium)	5.8	-281.63	431.27	3.53

3.2. Slow Strain Rate Tensile

The effect of salt exposure of alloys and their influence in the mechanical behavior of components in CSP plants is one of the main important topics to solve in the next generation of CSP plants. A better mechanical behavior was obtained in VM12 and T91, according with results showed in figure 7.

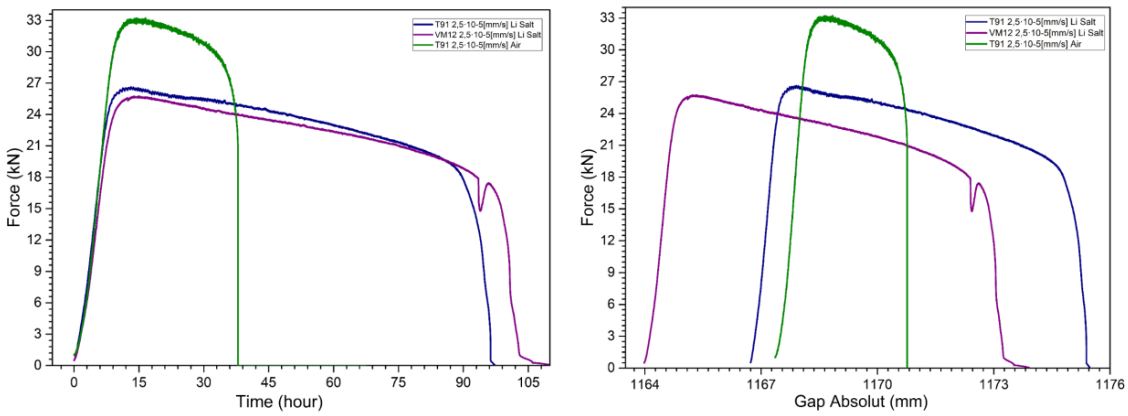

Fig. 7. SSRT results for VM12 and T91 steels immersed in ternary lithium salt

The results of the SSRT tests were carried out for the materials T91 and VM12. In the case of T91, it was carried out in molten salt for 7 days and in air for approximately 3 days. For the VM12 material, the test was performed in about 5 days. The tests were performed at a temperature of 550 ° C and a deformation rate of 2.5x10-5 mm / s (Figure 5). Due to a malfunction of the heating cycles, the air test of the material VM12 was not done. Other data were recorded manually, therefore, the graph for the sample tested in salt seems noisy.

In addition, it should be noted that the total voltage includes the elongation of the sample plus the elongation of the test device. Although the test bench has been isolated from the hot chamber and is equipped with chilled upper and base plates, it is possible that the heat flux differs between the salt and air tests due to the different heat and conductivity capacities of the different means, resulting in different contributions from the test bank to total displacement. Therefore, only strength in the performance and strength in the fracture should be compared. As it can be seen in Figure 5, the sample analyzed in air of the T91 material bears higher loads compared to the sample analyzed in salt. These tests have been carried out to test the principle of carrying out SSRT in molten salt with lithium content.

3.3. Flow Accelerated Corrosion

Figure 8 shows the degradation of the T91 material in both FAC (Flow Accelerated Corrosion) and static corrosion, in the form of weight loss, simulation operation condition in the pipeline. After 680 hours of corrosion under conditions of Flow corrosion and static corrosion there was no significant difference in the weight loss in the steel used.

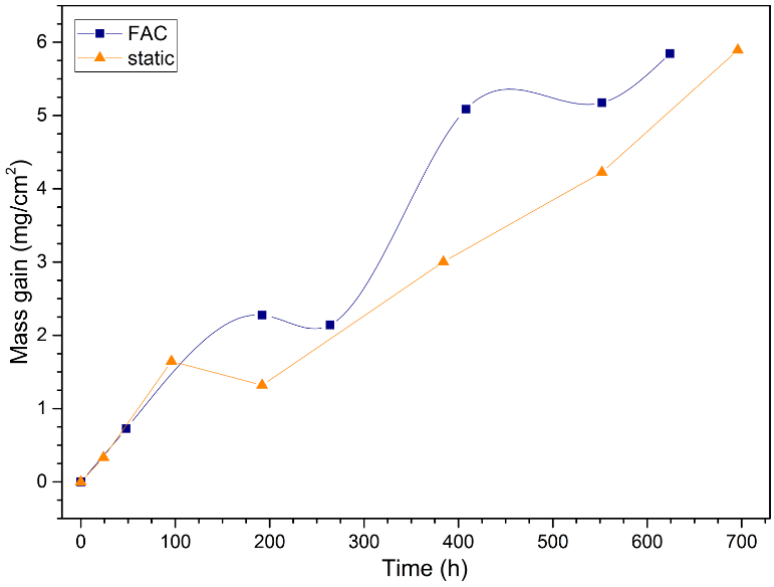

Fig. 8. FAC (Flow Accelerated Corrosion) and Static corrosion results for T91 steels immersed in ternary lithium salt

4. Conclusions

Electrochemical impedance spectroscopy (EIS) was applied to monitor the corrosion mechanism in molten salt with lithium content. The study of the corrosion in this mixture, allows us to compare the corrosion behaviour between the proposed salt of lithium content and other traditional techniques.

SSRT tests in the database are difficult to perform due to a corrosive attack on the test configuration. The SSRT configuration could be performed and the tests were successful. The interpretation of the results of the test is complex, since the multiple effects influence the sample during the test, for example: the samples need to endure corrosive attack from the salt and also at air at 550°C.

The flow velocity results mainly in an accelerated rate of cathodic reaction, by increasing the rate of oxygen diffusion. The velocity also affects the corrosion potential.

5. Acknowledgments

The authors would like to acknowledge the financial support provided by CONICYT / FONDAP 15110019 “Solar Energy Research Center” SERC-Chile. Fraunhofer IWM has received funding from the European Union’s Horizon 2020 research and innovation programme under grant agreement No. 686008.

6. References

Ahmed, W. H. (2010). Evaluation of the proximity effect on flow-accelerated corrosion. *Annals of Nuclear Energy*. https://doi.org/10.1016/j.anucene.2009.12.020

Bradshaw, R. W., & Goods, S. H. (2001). Corrosion Resistance of Stainless Steels During Thermal Cycling in Alkali Nitrate. *Sandia Report*, (SAND2001-8518), 1–39.

Cheng, W. J., Chen, D. J., & Wang, C. J. (2015). High-temperature corrosion of Cr-Mo steel in molten LiNO3-NaNO3-KNO3eutectic salt for thermal energy storage. *Solar Energy Materials and Solar Cells*, *132*, 563–569. https://doi.org/10.1016/j.solmat.2014.10.007

Ciucci, F. (2019). Modeling electrochemical impedance spectroscopy. *Current Opinion in Electrochemistry*, *13*, 132–139. https://doi.org/10.1016/j.coelec.2018.12.003

Fernández, Á. G., & Cabeza, L. F. (2019). Molten salt corrosion mechanisms of nitrate based thermal energy storage materials for concentrated solar power plants: A review. *Solar Energy Materials and Solar Cells*, *194*(February), 160–165. https://doi.org/10.1016/j.solmat.2019.02.012

Fernández, A. G., Galleguillos, H., & Pérez, F. J. (2014). Corrosion Ability of a Novel Heat Transfer Fluid for Energy Storage in CSP Plants. *Oxidation of Metals*, *82*(5–6), 331–345. https://doi.org/10.1007/s11085-014-9494-3

Gauché, P., Rudman, J., Mabaso, M., Landman, W. A., von Backström, T. W., & Brent, A. C. (2017). System value and progress of CSP. *Solar Energy*, *152*, 106–139. https://doi.org/10.1016/j.solener.2017.03.072

Gomez-Vidal, J. C., Fernandez, A. G., Tirawat, R., Turchi, C., & Huddleston, W. (2017). Corrosion resistance of alumina-forming alloys against molten chlorides for energy production. I: Pre-oxidation treatment and isothermal corrosion tests. *Solar Energy Materials and Solar Cells*, *166*(January), 222–233. https://doi.org/10.1016/j.solmat.2017.02.019

Green, A., Diep, C., Dunn, R., & Dent, J. (2015). High Capacity Factor CSP-PV Hybrid Systems. *Energy Procedia*, *69*, 2049–2059. https://doi.org/10.1016/j.egypro.2015.03.218

McConohy, G., & Kruizenga, A. (2014). Molten nitrate salts at 600 and 680°C: Thermophysical property changes and corrosion of high-temperature nickel alloys. *Solar Energy*, *103*, 242–252. https://doi.org/10.1016/j.solener.2014.01.028

Mehos, M., Turchi, C., Vidal, J., Wagner, M., Ma, Z., Ho, C., … Kruizenga, A. (2017). *Concentrating Solar Power Gen3 Demonstration Roadmap*. https://doi.org/10.2172/1338899

Preußner, J., Pfeiffer, W., Piedra, E., Oeser, S., Tandler, M., Von Hartrott, P., & Maier, C. (2016). Long-term material tests in liquid molten salts. *Advances in Materials Technology for Fossil Power Plants*, 1126–1137.

Starke, A. R., Cardemil, J. M., Escobar, R. A., Lemos, L. F. L., & Colle, S. (2015). Assessing the performance of

Concentrated Solar Power plants in selected locations of Chile. *Proceedings of ECOS 2015 - The 28th International Conference on Efficiency, Cost, Optimization, Simulation and Environmental Impact of Energy Systems*.

Stekli, J. (2013). *Technical Challenges and Opportunities for Concentrating Solar Power With Thermal Energy Storage*. *5*(June), 1–12. https://doi.org/10.1115/1.4024143

Zeng, C. L., Wang, W., & Wu, W. T. (2001). Electrochemical impedance models for molten salt corrosion. *Corrosion Science*, *43*(4), 787–801. https://doi.org/10.1016/S0010-938X(00)00108-6